RESEARCH PAPER

The investigation on different light harvesting layers and their sufficient effect on the photovoltaic characteristics in dye sensitized solar cell

Mohammad Mazloum-Ardakani *, Rezvan Arazi

Department of Chemistry, Faculty of Science, Yazd University, Yazd, Iran

ARTICLE INFO

Article History:
Received 17 October 2016
Accepted 23 December 2016
Published 15 January 2017

Keywords:
Dye sensitized solar cell
Electrospinning
Sol–gel
TiO_2 nanofibers
TiO_2 nanoparticles

ABSTRACT

Titanium dioxide-based nanofibers (TiO_2 nanofiber) were prepared by an electrospinning technique. The electrospun composite fibers were synthesized at different concentrations of titanium isopropoxide (25.35, 50.69, 76.05 wt%) and calcinated at different temperatures (450 °C, 650 °C and 850 °C) for 2 h. The diameters of nanofibers decreased by increasing the inorganic part of composite nanofibers and principally depicted anatase, anatase- rutile and rutile phases. By increasing temperature from 450 °C to 850 °C, the anatase phase decreased whereas the rutile phase increased. The different optimized TiO_2 nanofibers were prepared and utilized as a sufficient scattering layer for the photoanode in dye sensitized solar cells. Then, the electron transport and recombination in TiO_2 nanofiber based dye sensitized solar cells (DSSCs) was investigated. It was shown that the electron life time in DSSCs with TiO_2 nanofibers, as a scattering layer, increases in different photoanode electrodes compared to that on DSSCs based on nanoparticles. As a result, conversion efficiency of 5.6% is realized, which is 55.37% higher than TiO_2 photoanodes without addition of nanofibers as a scattering layer.

How to cite this article
Mazloum-Ardakani M, Arazi R. The investigation on different light harvesting layers and their sufficient effect on the photovoltaic characteristics in dye sensitized solar cell. Nanochem Res, 2017; 2(1): 20-28. DOI: 10.22036/ncr.2017.01.003

INTRODUCTION

Recently, titanium dioxide materials have been utilized in many fields such as dye sensitized solar cell [1,2], photocatalysis [3] and electrochemical measurements [4,5]. The main advantages of TiO_2 nanomaterials are unique physical, chemical properties, the high surface to volume ratio and crystalline structure. TiO_2 nanostructure preparation with unique properties such as hydrothermal synthesis [6], sol gel process [7], atomic layer deposition [8], reactive sputtering [9] has been expanded during past decay. However, extensive studies in this respect show that the nanostructures with one-dimensional shape (1D) have special features due to the axial ratio aspect [10]. Among the 1D shape, nanofibers have obtained much interest due to long axial ratio, large surface area to volume and flexibility in surface functionalities. Recently, electrospinning process was used as a low cost and fast technology to product fibers with diameters in the range of 3 nm to greater than 10 μm [11]. It proposes significant capabilities to synthesize nanofibers by controllable morphology with optimized conditions such as smaller diameter and higher surface area compared to the regular fibers. Nanofibers have been successfully applied in in a wide range of areas including filtration of air and water, tissue engineering scaffolds, biomedical and bio technology [12–14].

During the electrospinning, a polymer solution flows out from needle connected to a syringe,

* Corresponding Author Email: *mazloum@yazd.ac.ir*

and a high voltage causes that the charge to be induced within the polymer and polymer pulled onto a collector by strong electric field and form nanofibers structure. Many parameters influence on final nanofibers structure, such as (1) solution conditions (2) operation conditions and (3) ambient conditions [15–17].

Dye sensitized solar cells DSSCs, a new type of photo-electrochemical solar cells, have been gained important alternative to the silicon based photovoltaic because they have significant benefits such as low cost, simple preparing processes and higher conversion efficiency in comparison of other types of solar cell. In recent years, one dimensional electrospun TiO_2 nanofibers have been used as the DSSC photoanode to enhance the electron transport and the light harvest efficiency by scattering more light in the red part of the solar spectra.

In this study, we synthesized TiO_2 nanofibers by optimization of electrospinning parameters such as polymer concentration, applied voltage, the distance between tip and collector, the calcinating temperature and the titanium isopropoxide concentrations to prepare TiO_2 nanofibers with high roughness surface and utilize them in photoanode to investigate the effect of fibers morphology on dye sensitized solar cell performance.

EXPERIMENTAL

Materials

Iodine (99.99%, Merck), lithium iodide (Merck), ethyl celluloses (30–50 mPas, Sigma Aldrich), terpineol (anhydrous, Sigma Aldrich), 4-tert-butylpyridine (4-tBP) (Sigma Aldrich), acetonitrile (Sigma Aldrich), valeronitrile (Sigma Aldrich), chloroplatinic acid hexahydrate (H_2PtCl_6) (Merck), and Ru complex dye [Dyesol, cis-bis(isothiocyanato) bis(2,2-bipyridyl-4,4-dicar-boxylato)-ruthenium(II) bis-tetra butyl ammonium: (N719)] were used as received. $TiCl_4$ (Sigma Aldrich) was diluted with water to 2.0 M at 0 °C which was used freshly and diluted to 40 mM with water for each treatment of the fluorine-doped tin oxide (FTO) (TEC-15, Dyesol) coated glass plates and surfaces of TiO_2 mesoporous electrodes. Polyvinyl pyrrolidone (PVP, M_w =1300000) was dissolved in 4 mL ethanol (EtOH, Merck, 99.8%) and 1 mL N, N-dimethylformamide (DMF, Merck, 99.8%).

Preparation of Titanium Dioxide Nanofibers

A solution of titaniumisopropoxide ($Ti(OCH(CH_3)_2)_4$, TiP, Aldrich,) with the metal contents of 25.35, 50.69, 76.05 wt% were prepared by stirring and 3 mL acetic acid was added to the solution until a transparent solution was obtained. Then, the titanium dioxide sol was added into polyvinyl pyrrolidone (PVP) solution while stirring for 6 h to obtain suitable viscosity. The obtained spinable sol was injected by a 5 mL plastic syringe (diameter: 12.08 mm). A power supply with high voltage (EH-Series, Glassman High Voltage) influence on the prepared Titania sol that is flowed toward a cylindrical target with an aluminum (Al) foil. The distance between the Al foil and the spinneret and the applied voltage were 15 cm and 15 KV respectively. A flow rate of 0.5 mL/h was utilized with a syringe pump (FNM Co., Iran). The nanofibers were deposited on the Al foil and then dried at 70 °C for 6 h to evaporate their solvents. Then, the prepared Titania nanofibers were divided into three parts and calcined in different temperatures (450 °C, 650 °C, 850 °C) at the rate of 2 °C/min for 2 h and utilized as light harvesting layers in dye sensitized solar cells photoanode.

Preparation of Electrodes and DSSCs Assembly

A TiO_2 nanoparticle paste was synthesized and covered on a FTO glass by the doctor Blade technique. Before using FTO as a substrate, it was first cleaned by distilled water, ethanol, and acetone for 20 min and then treated by 40 mM $TiCl_4$ (30 min at 80 °C). The counter electrodes were cleaned by distilled water and HCl (0.1 M) in ethanol. Then, the FTO-TiO_2 paste heated at 450 °C for 15 min to enhance electrical contact and adhesion (TiO_2 electrode). The dye sensitized solar cells were prepared by immersing 0.09 cm^2 calcined TiO_2 electrode in a 0.5 mM Ruthenium-based N719 dye for 32 h at room temperature. The dye sensitized nanoparticle/nanofiber electrodes were dried and used immediately for measurement of their photovoltaic properties. Photovoltaic measurements were performed under 1 sun conditions (100 $mWcm^{-2}$). The cells were sealed using a 0.5 mm wide strips of 60 mm thick surlyn and an iodide based electrolyte with 0.03 M Iodine (I_2), 0.1 M LiI and 0.5 M 4-tBP in the 5 mL of acetonitrile: valeronitrile (85:15) was injected into the cell. After covering the holes with small cover glasses they were sealed and used to measure photovoltaic performance.

Characterizations

The structure of titanium dioxide nanofibers were characterized using X-ray diffractometer (Xpert Pro MPD model, wavelength of Cu K radiation

in 2 range 10-80). Scanning electron microscopy (SEM) images of different nanofibers calcined in different temperatures, were taken out by TESCAN instrument model VEGA3. The infrared (IR) spectra of the electrospun nanofibers were done with a Bruker instrument model 55. UV-Vis of dye solutions and dyes adsorbed on TiO_2 surface was performed by a spectrophotometer Optizen model 3220 from 200 to 900 nm wavelengths using a glass cuvette with 1 cm path length.

RESULTS AND DISCUSSION

Material Characterization

XRD analysis was performed to find the crystalline phase of the prepared nanofibers in different calcinating temperatures. The results for the heat-treated samples are depicted in Fig. 1. As it is found from the XRD pattern, heated fibers at 450 °C for 1 h leads to formation of a white residue which is the crystalline TiO_2 nanofibers in anatase phase. The obtained spectrum after heat treatment at 450 °C in air has the TiO_2 anatase phase peaks at 2θ = 25.3, 37.7, 47.8, 54, 62.7, 68.6, 70.3, and 75.2. These results are in good agreement with previous reports [18]. In the other words, when the heating rate was fast (5 °C/min), anatase titanium was formed after calcination at 450 °C Fig. (1A). It was found that all the sharp features observed at 2θ = 25.3, 37.0, 38.37, 47.9, 54, 55.21, 62.7, 68.6 and 70.08 in the XRD pattern are consistent with anatase (101), (004), (112), (200), (105), (211), (204), (220), (220) and (215) degrees with no impurity which is in agreement with 21-1272 standard cards from JCPDS. The prominent peaks representing anatase/rutile phase of nanocrystalline TiO_2 powder at 650 °C used for this study can be seen at the 2θ values of 25.28, 27.48, 37.80, 48.05, 53.89, 55.06, 62.69, 68.76, 70.31 and 75.03 Fig. (1B). On the heating rate and temperature the crystal structures of the nanofibers can therefore be manipulated to yield distinct properties from the same starting materials. On the other hand, when the solution was slowly heated (0.5 °C/min) and calcined at 850 °C, rutile Titania resulted in Fig. (1C). The XRD features (101), (110), (111), (200), (211), (220), (002), (310) and (301) can be indexed to the rutile Titania crystal with the sharp features observed at 2θ = 25.09, 27.45, 39.5, 41.4, 55.21, 56.3, 64, 65.3 and 69.1. Fig. 2 (A) shows the FT-IR spectra of TiO_2 nanofibers in a region of 400–4000 cm^{-1}. The presence of a heteroatom and a carbonyl group in the pyrrolidone ring sufficiently reduces the symmetry [19] as shown in Fig. 2 (A). The sharp peak at 1632 cm^{-1} corresponds to the stretching vibration of carboxyl group, which is a typical mode of PVP, while the absorption band around 2923 cm^{-1} can be attributed to the C–H stretching vibrations [19]. In addition, it can be clearly seen that the composite nanofibers contain a trace hydroxyl group due to the electrospun solution. A broad stretching band at about 3426 cm^{-1} appears in the composite nanofibers, which can be assigned to the vibration of the associated hydroxyl groups. As shown in Fig. 2 (B), the FT-IR spectra of nanofibers with 50.69 wt% of TiP is recorded in the range of 400-4000 cm^{-1} calcined at different temperature. In the spectra of the samples calcined at 450 °C, the bands associated with the vibration mode of the skeletal O-Ti-O bonds of anatase phase appeared at 404 cm^{-1} (Fig. 2B (a)), and several components not well resolved in the range of 550 to 900 cm^{-1} [20]. After calcination at 650 °C for 2 h (Fig. 2B (b)), there was a shift of the main anatase band from 404 to 500 cm^{-1} and a new band appeared at around 700 cm^{-1}. The shift of the main

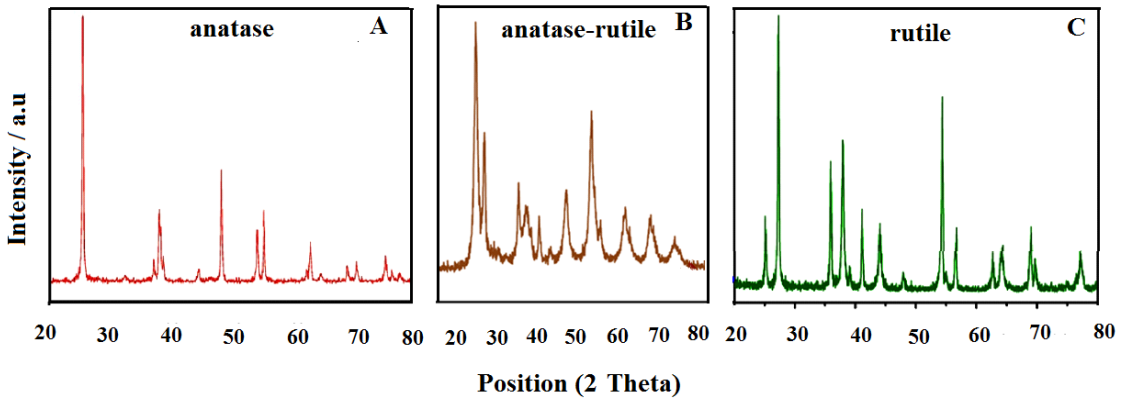

Fig. 1. Effect of different calcinating temperatures on the crystal structure of TiO_2 nanofibers

adsorption at 404 cm^{-1} has been generally attributed to variations in particle size and morphology. Within increasing the calcination temperature to 850 °C, the appearance of the band near 700 cm^{-1} with higher intensity (Fig. 2(c)) was associated with the TiO_2 rutile phase [20]. These results also showed the anatase to rutile transformation occurred at this temperature. Fig. 3 (A)-(F) shows the SEM images of electrospun nanofibers TiO_2 nanofibers with different concentrations of $Ti(OCH(CH3)_2)_4$ (25.32, 50.69 and 76.05 wt%) and heat-treatment conditions. The images in Fig. 3 (A, B) indicate that the average diameter of the electrospun TiO_2 nanofibers significantly decreases as the amount of TiO_2 increases. As mentioned before, TiO_2 nanofibers were generated after the calcination of electrospun Ti(IV) isopropoxide/PVP nanofibers. Low and high resolution SEM images of 50.69 wt% before and after calcination at different temperatures are shown in Fig. 3 (D-F). The as prepared composite nanofibers were straight with smooth surface, Fig. 3 (A). Increasing the amount of TiP resulted in decreasing the diameter of nanofibers, Fig. 3 (B). After calcinations at different temperatures also the nanofibers retained their fibrous structure. However, when the temperature was too high, the anatase phase transform to rutile phase.. The observation depicts that the morphology of samples is irregular and rough due to the crystal grains of the titanium dioxide and may be beneficial to enhance the dye adsorbing due to its great surface roughness and high surface area. The average diameter of calcined fibers was smaller than that of electrospun non-calcined fibers because of the decomposition of organic components by increasing the temperature. The

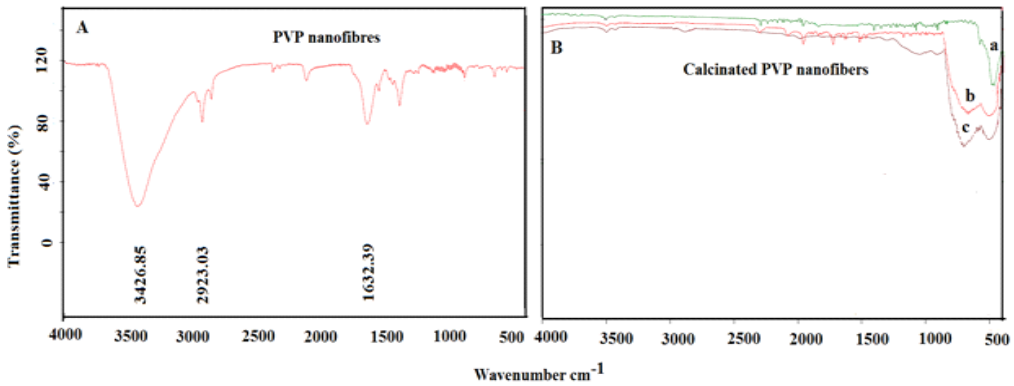

Fig. 2. FT-IR spectra of nanofibers with 50.69 wt% of TiP before (A) and after calcination (B) in different temperatures (a) 450 °C, (b) 650 °C, (c) 850 °C

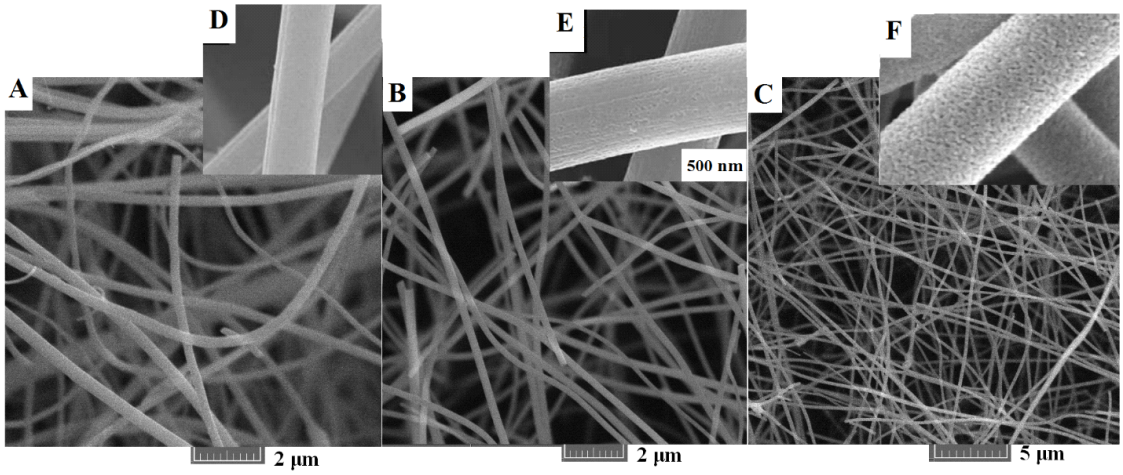

Fig. 3. SEM images of nanofibers with different concentrations of TiP (A-C) calcined at different temperatures. (D) 450 °C; (E) 650 °C; (F) 850 °C

schematic description of Scheme 1 seems to be consistent with the SEM images at different calcinating temperatures (Fig. 3).

Evaluation of DSSC performance

Optical Properties

The photoanode electrodes were fabricated in four different manners and utilized as a scattering layer. (1) After blading the block layer on the surface of FTO glass, the TiO_2 paste with particle size of 20-30 nm was bladed on the surface as the blocking layer (BNP. Standard sample), the TiO_2 paste with particle size of 400 nm was bladed on the surface of the blocking layer (bladed nanoparticles paste scattering layer, BNS), (2) The prepared electrospun nanofiber was dissolved in 0.5 mM $TiCl_4$, heated at 80 ºC temperature for 30 min and exposed on the blocking layer (nanofibers $TiCl_4$ post-treatment scattering layer, NTS), (3) The electrospun nanofiber was dissolved in 0.5 mM $TiCl_4$ and exposed on the blocking layer by sputtering (sputtered nanofibers scattering layer, SNS), (4) TiO_2 paste with particle size of 400 nm was mixed by TiO_2 nanofibers and bladed on the surface of blocking layer (mixed nanoparticles and nanofibers scattering layer, NPFS). Fig. 4 displays the UV-Vis absorption spectra of the N719 dye and dye sensitized different photoanode electrodes in diluted ethanol solution. Metal-to-ligand charge-transfer is displayed with two broad visible bands at 540 and 395 nm in dye. The bands at 310 nm with a shoulder at 300 nm are attributed to intra ligand (π-π*) charge-transfer transitions [21]. By adsorbing dye on TiO_2 surface, the dye absorption spectra are broadened and blue-shifted more or less as compared to that in solutions because of H-type aggregation of the dye on the TiO_2 surface [22]. As obviously seen in this figure, the combination of TiO_2 paste and TiO_2 nanofibers with high surface area absorbed more dye than regular TiO_2 nanoparticles sufficiently. In the other words, the concentration of dye molecules on the combined scattering layer is more than those on the other types of regular prepared layer, indicating improvement in the optical absorption efficiency of the dye molecules, resulting in increasing in the photocurrent density and carrier transport properties of the photoanode.

Photovoltaic Performance and EIS Analysis

Photocurrent density versus voltage features of DSSCs based on the nanoparticle electrode alone and the nanoparticle/nanofiber electrode are depicted in Fig. 5 and Table 1. For the TiO_2 nanoparticle electrode without nanofibers, the short-circuit photocurrent density, J_{sc}, and the conversion

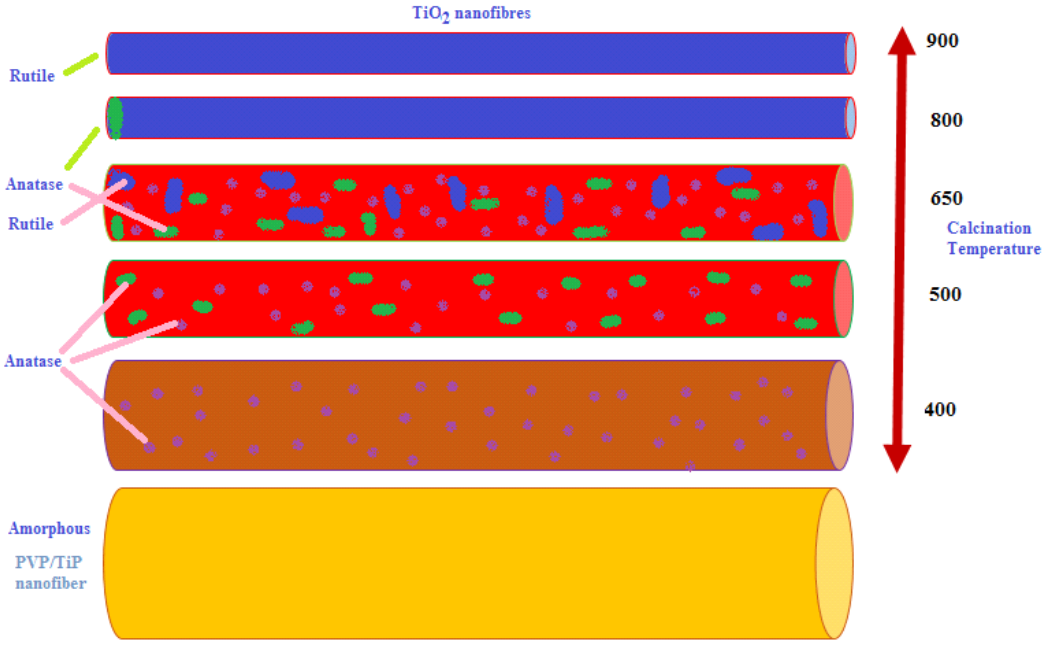

Scheme 1. Schematic illustration of phase transformation of TiO_2 nanofibers at different calcination temperatures

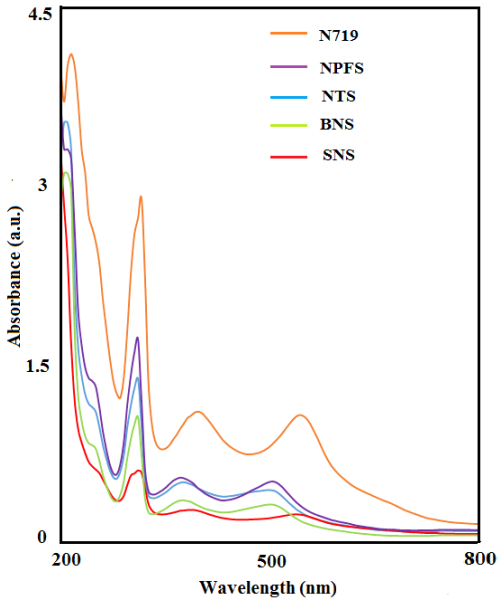

Fig. 4. UV-Vis absorption spectra of the absorbed dye molecules (N719 dye) on different photoelectrodes of TiO_2 nanofibers

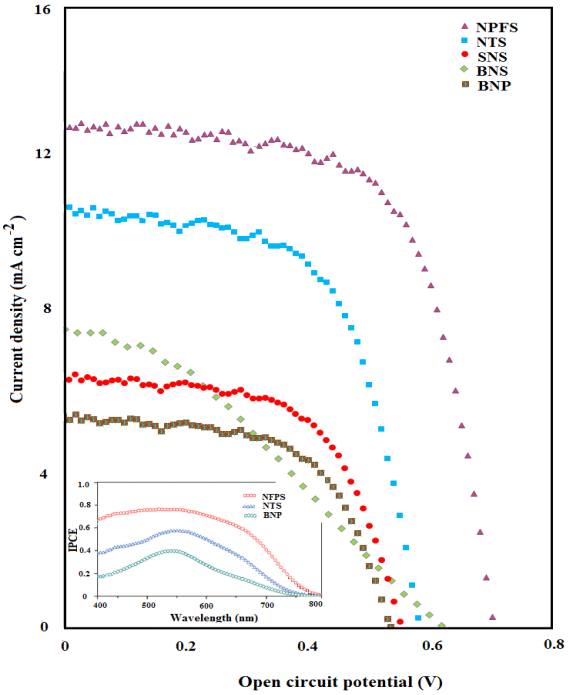

Fig. 5. J-V curves of different photoanode electrodes. The inset is IPCE spectra of DSSC constructed with BNP, TNS and NFPS

efficiency η of the TiO_2 nanoparticle cell were known to be decreased. The addition of large nanoparticles on the top of photoelectrode, acting as light-harvesting layers, was also reported previously [23]. In comparison with the nanoparticle, the special properties of nanofibers such as well aligned and nanofibrils in one-dimension might resulted in enhancing the charge transfer because of fewer grain boundaries. While mixing nanoparticles and nanofibers to prepare scattering layer, significant penetration of the electrolyte into the TiO_2 nanoparticle/nanofiber electrode occurs by increased porosity. Because of increasing the amount of adsorbed dye molecules on the electrode surface as compared with the only nanoparticle cell. The J_{sc} for nanofiber/nanoparticle cells enhanced significantly. The enhanced current density obtained with TiO_2 nanoparticles/nanofibers was due to sufficient light harvesting by TiO_2 films. Higher surface area of combined nanoparticles/ nanofibers layer improved the anchoring of more dye molecules on the surface of TiO_2 scattering layer, leading to a significant optical absorbance.

The IPCE results (quantum efficiency) of device fabricated by bladed nanoparticles paste blotching layer, BNP, (nanofibers $TiCl_4$ post-treatment scattering layer, NTS, and mixed nanoparticles and nanofibers scattering layer, NPFS, are shown in Fig. 5 (inset). The maximum efficiency for nanoparticles and nanofibers containing cell was over 68% at 550 nm that was increased from 41.4 % to 68 % at 550 nm by NPFS based cells. The enhancement of ~27% suggests that the mixed nanoparticles and nanofibers scattering layer based devices have more electron injection and better electron transportation treatment than those of the bladed nanoparticles paste blotching layer. The NPFS film having large surface area prepared by electrospinning technique could be one possible solution to the high efficiency electron conductor in the DSSCs.

The advantages of this work in comparison with others are optimizing the electrospinning

Table 1. Photovoltaic parameters for different photoanode electrodes

Electrode types	V_{oc}	J_{sc}	FF(%)	η (%)	τ_r
NFPS	0.71	12.63	64	5.6	6.4
BNS	0.62	7.45	54	2.5	4.7
NTS	0.58	10.56	62	3.95	3.4
SNS	0.55	6.29	60	2.08	1.5
BNP	0.53	5.4	59	1.7	1.2

parameters, the value of Tip and the efficient calcination temperature to obtain roughness and desirable diameters of nanofibers that are utilized for scattering layer, preparation different scattering layer by variable methods (BNP, BNS, NTS, SNS, and NPFS), the effect of different temperatures on phase changes (by increasing the temperature, the phase of nanofibers changes from anatase to rutile) and the study on their sufficient effect on the dye sensitized solar cell performance [24–29].

The conversion efficiency of DSSC using TiO_2 nanoparticles/nanofibers was about 2 times higher than that of DSSC using regular TiO_2 nanoparticles. The improved energy conversion efficiency was principally from the increase in J_{sc} compared to that for regular nanoparticles based DSSCs, indicating that nanofibrous structure makes the electron injection density easer through sufficient interface between dye molecules and nanoparticle/nanofiber scattering layers. The higher surface area is assigned to the larger amount of adsorbed dyes. Open circuit potential, $V_{oc,}$ is attributed to the energy gap between Fermi level of semiconductor and Nernst potential of I^-/I_3^- couple. It is affected by the electron affinity of semiconductor and ionization potential of dye. The reduction in charge recombination and the negatively shift of semiconductor conduction bond resulting in higher open circuit voltage. The improved V_{oc} for the combined TiO_2 nanoparticles/nanofibers photoanode in DSSC is attributes to the facile penetration of electrolyte into TiO_2 electrode surface, which retarded back electron transfer and enhanced the redox process between dye oxide cation and redox couple in electrolyte. The existence of mesoporous morphology in combination with nanofibrous web led to the better contact with electrolyte, and adsorption of dye molecules on the nanoparticles/nanofibers electrode surface were increased significantly. Undoubtedly, the increased efficiency aroused by the application of nanofibers as the scattering layer in TiO_2 –electrode (photoanode) is attributable to the large surface area, which favors the adsorption of a large amount of dye molecules, as well as a high scattering effect for visible light. The results are summarized in Fig. 6.

Electrochemical impedance spectroscopy (EIS) was carried out at V_{oc} to understand the improved transfer of electrons in solar cells with different TiO_2 photoanodes under 1 sun illumination. The spectra are shown in Fig. 7 for different cells with

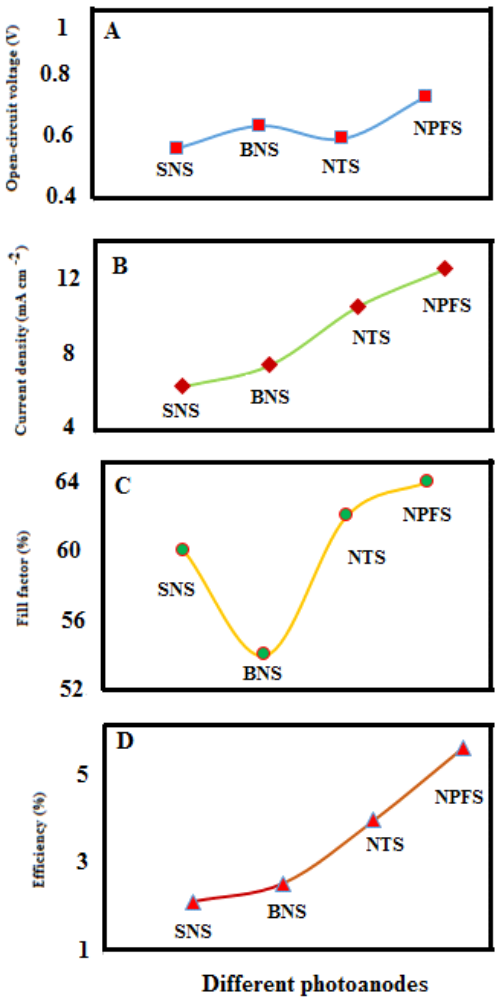

Fig. 6. Photovoltaic-characteristics relationship with different TiO_2 photoanodes (A) V_{oc}, (B) J_{sc}, (C) FF, and (D) η, respectively.

nanoparticles and nanofibers scattering layers. Two semicircles, including a small one at high frequency and a large semicircle at low frequency, were observed in the Nyquist plots (Fig. 7). The small semicircle at high frequency corresponds to the I^-/I_3^- reaction at the Pt-counter electrode, and the larger one at low frequency is assigned to the injection/recombination reactions and electron diffusion in the TiO_2 electrode. With a fitting program using Z view software, these data were analyzed. The equivalent circuit used for fitting the impedance spectra of the DSSC is shown in the inset of Fig. 7. In a simple equivalent circuit [30], R_s, R_{CE}, R_{ct} and R_w are known as series resistance, charge transfer resistance at the counter electrode/electrolyte interface, electron recombination resistance at the dyed-TiO_2/electrolyte interface

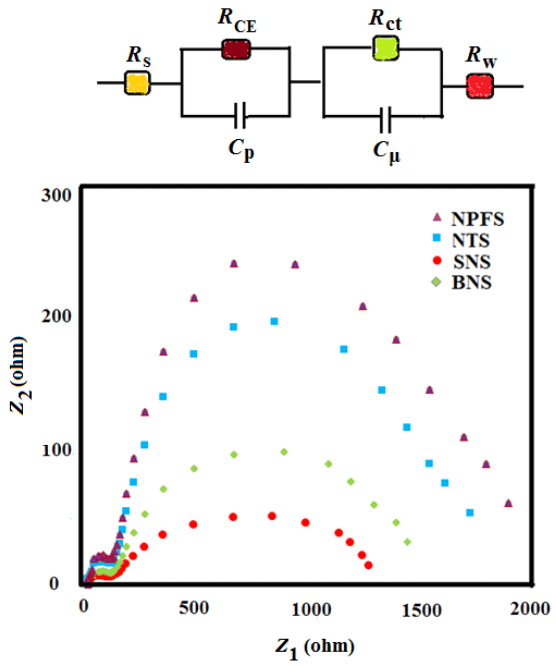

Fig. 7 EIS spectra of different photoanode electrodes

and Nernst diffusion impedance, respectively. C_p and C_μ are assigned to the chemical capacitance at the dyed-TiO_2/electrolyte interface and the counter electrode/electrolyte interface, respectively. Due to the low frequency (f_{min}) characteristic of the diffusion coefficient, the electron life time (τ_r) can be calculated using $\tau_r = 1/ (2\pi f_{min})$ [31]. In the case of the nanoparticles/nanofiber cell, the electron life time was calculated to be 6.4 ms compared to 4.7 ms estimated for the BNS, 3.4 ms NTS and 1.5 ms SNS sample. The low value of electron life time depicts the increase in charge recombination between the electrons in conduction bond returned back to the electrolyte. Because of the existence of a higher transport resistance accompanied by a low electron life time, the dark current enhanced which leads to lower V_{oc} and η. As it is found from the figure, at different prepared scattering layers the second semicircle in mixing nanoparticles and nanofibers is larger than only nanoparticles, resulting the improvement in charge recombination resistance and significant enhance in V_{oc} and J_{sc}. When the charge recombination occurred, the electron density was reduced in the TiO_2 layer and resulted in decreasing R_{ct}. More electron accumulation in the TiO_2 layer can cause to shift upward the electron quasi-Fermi level and to increase V_{oc} consequently.

CONCLUSION

The TiO_2 nanofibers with different diameters and calcination temperature and $Ti(OCH(CH3)_2)_4$ concentration were prepared using electrospun fibers of TiO_2/PVP. The experimental results showed that uniform, rough and continuous fibers with decreased diameters are observed for the electrospun fibers containing a $Ti(OCH(CH3)_2)_4$ concentration of 50.69 wt% at a flow rate of 0.5 mL/h, and an electric field of 15 kV/cm and 850 °C. FT-IR results also showed the formation of anatase- rutile titanium dioxide at 650 °C and its transformation into rutile phase at 850 °C. The calcined and optimized nanofiber substrates were used in the fabrication of dye-sensitized solar cell as the different photoanodes. Among different prepared scattering layers, the combination of nanofibers and nanoparticles has the most values for V_{oc}, J_{sc} and efficiency because of its high surface area, large amount of anchored dye and larger charge recombination resistance. These results suggest that light harvesting nanofibers-modified nanoparticles are very promising materials for the electrode structure of dye sensitized solar cell. The result clearly demonstrates that large surface area of semiconducting materials are necessary to prepare effective light and dye absorption, for better electrical connection with redox electrolytes, crystallinity and the photocurrent density, when TiO_2 paste with particle size Titania is observed.

ACKNOWLEDGMENTS

The authors wish to thank the Yazd University Research Council, IUT Research Council and Excellence in Sensors for financial support of this research.

CONFLICT OF INTERESTS

The authors declare that there is no conflict of interests regarding the publication of this paper.

REFERENCES

1. Mathew S, Yella A, Gao P, Humphry-Baker R, CurchodBasile FE, Ashari-Astani N, et al. Dye-sensitized solar cells with 13% efficiency achieved through the molecular engineering of porphyrin sensitizers. Nat Chem. 2014;6(3):242-7.
2. Mazloum-Ardakani M, Khoshroo A. Enhanced performance of dye-sensitized solar cells with dual-function coadsorbent: reducing the surface concentration of dye-iodine complexes concomitant with attenuated charge recombination. Physical Chemistry Chemical Physics. 2015;17(35):22985-90.
3. Ojani R, Raoof J-B, Khanmohammadi A, Zarei E. Photoelectrocatalytic degradation of 3-nitrophenol at surface of Ti/TiO2 electrode. Journal of Solid State

Electrochemistry. 2013;17(1):63-8.

4. Mazloum-Ardakani M, Arazi R, Naeimi H. Preparation of TiO2 Nanoparticles/2, 2′-(1, 3-propanediylbisnitrilo-ethylidine) bis-Hydroquinone Carbon Paste Electrode and Its Application for Simultaneous Sensing of Trace Amounts of Ascorbic acid, Uric acid and Folic acid. Int J Electrochem Sci. 2010;5:1773-85.
5. Mazloum-Ardakani M, Khoshroo A. Nano composite system based on coumarin derivative–titanium dioxide nanoparticles and ionic liquid: Determination of levodopa and carbidopa in human serum and pharmaceutical formulations. Analytica Chimica Acta. 2013;798:25-32.
6. Nian J-N, Teng H. Hydrothermal Synthesis of Single-Crystalline Anatase TiO2 Nanorods with Nanotubes as the Precursor. The Journal of Physical Chemistry B. 2006;110(9):4193-8.
7. Su C, Hong BY, Tseng CM. Sol–gel preparation and photocatalysis of titanium dioxide. Catalysis Today. 2004;96(3):119-26.
8. Aarik J, Aidla A, Mändar H, Uustare T. Atomic layer deposition of titanium dioxide from TiCl4 and H2O: investigation of growth mechanism. Applied Surface Science. 2001;172(1):148-58.
9. Lindgren T, Mwabora JM, Avendaño E, Jonsson J, Hoel A, Granqvist C-G, et al. Photoelectrochemical and Optical Properties of Nitrogen Doped Titanium Dioxide Films Prepared by Reactive DC Magnetron Sputtering. The Journal of Physical Chemistry B. 2003;107(24):5709-16.
10. Greiner A, Wendorff JH. Electrospinning: A Fascinating Method for the Preparation of Ultrathin Fibers. Angewandte Chemie International Edition. 2007;46(30):5670-703.
11. Subbiah T, Bhat GS, Tock RW, Parameswaran S, Ramkumar SS. Electrospinning of nanofibers. Journal of Applied Polymer Science. 2005;96(2):557-69.
12. Li D, Xia Y. Fabrication of Titania Nanofibers by Electrospinning. Nano Letters. 2003;3(4):555-60.
13. Peng Y-T, Lo C-T. Electrospun porous carbon nanofibers as lithium ion battery anodes. Journal of Solid State Electrochemistry. 2015;19(11):3401-10.
14. Yuan Z-Y, Su B-L. Titanium oxide nanotubes, nanofibers and nanowires. Colloids and Surfaces A: Physicochemical and Engineering Aspects. 2004;241(1):173-83.
15. Matthews JA, Wnek GE, Simpson DG, Bowlin GL. Electrospinning of Collagen Nanofibers. Biomacromolecules. 2002;3(2):232-8.
16. Bognitzki M, Czado W, Frese T, Schaper A, Hellwig M, Steinhart M, et al. Nanostructured Fibers via Electrospinning. Advanced Materials. 2001;13(1):70-2.
17. Doshi J RDH. In Electrospinning Process and Applications of Electrospun Fibers. Ind Appl Soc Annu Meet1993. p. 1698-703.
18. Jarusuwannapoom T, Hongrojjanawiwat W, Jitjaicham S, Wannatong L, Nithitanakul M, Pattamaprom C, et al. Effect of solvents on electro-spinnability of polystyrene solutions and morphological appearance of resulting electrospun polystyrene fibers. European Polymer Journal. 2005;41(3):409-21.
19. Zhang C, Yuan X, Wu L, Han Y, Sheng J. Study on morphology of electrospun poly(vinyl alcohol) mats. European Polymer Journal. 2005;41(3):423-32.
20. Ocaña M, Fornés V, Ramos JVG, Serna CJ. Factors affecting the infrared and Raman spectra of rutile powders. Journal of Solid State Chemistry. 1988;75(2):364-72.
21. Kawano R, Nazeeruddin MK, Sato A, Grätzel M, Watanabe M. Amphiphilic ruthenium dye as an ideal sensitizer in conversion of light to electricity using ionic liquid crystal electrolyte. Electrochemistry Communications. 2007;9(5):1134-8.
22. Menzies D, Cervini R, Cheng Y, Simon G, Spiccia L. Titanium Isopropoxide Post-Treatment of Titanium Dioxide Electrodes for use in Dye-Sensitised Solar Cells. Journal of the Australasian Ceramic Society. 2003;39(2):108-13.
23. Zhang X, Thavasi V, Mhaisalkar SG, Ramakrishna S. Novel hollow mesoporous 1D TiO2 nanofibers as photovoltaic and photocatalytic materials. Nanoscale. 2012;4(5):1707-16.
24. Chuangchote S, Sagawa T, Yoshikawa S. Efficient dye-sensitized solar cells using electrospun Ti O 2 nanofibers as a light harvesting layer. Applied Physics Letters. 2008;93(3):266.
25. Francis L, Sreekumaran Nair A, Jose R, Ramakrishna S, Thavasi V, Marsano E. Fabrication and characterization of dye-sensitized solar cells from rutile nanofibers and nanorods. Energy. 2011;36(1):627-32.
26. Kim Y-H, Lee I-K, Song Y-S, Lee M-H, Kim B-Y, Cho N-I, et al. Influence of TiO2 coating thickness on energy conversion efficiency of dye-sensitized solar cells. Electronic Materials Letters. 2014;10(2):445-9.
27. Park YD, Anabuki K, Kim S, Park K-W, Lee DH, Um SH, et al. Fabrication of stable electrospun TiO2 nanorods for high-performance dye-sensitized solar cells. Macromolecular Research. 2013;21(6):636-40.
28. Mathew A, Gowravaram MR, Nookala M. Application of mesoporous anataseTiO2 microspheres for dye sensitized solar cell on flexible titanium metal photo anode. Advanced materials letters. 2013;4(10):737.
29. Li J, Xu W, Shi Y. TiO2 nanofiber based dye sensitized solar cells with improved carrier collection efficiency. Transaction on Control and Mechanical Systems. 2012;1(6).
30. Hauch A, Georg A. Diffusion in the electrolyte and charge-transfer reaction at the platinum electrode in dye-sensitized solar cells. Electrochimica Acta. 2001;46(22):3457-66.
31. Kern R, Sastrawan R, Ferber J, Stangl R, Luther J. Modeling and interpretation of electrical impedance spectra of dye solar cells operated under open-circuit conditions. Electrochimica Acta. 2002;47(26):4213-25.